Check for updates

ChemElectroChem

Perspective
doi.org/10.1002/celc.202500051

Chemistry Europe
European Chemical Societies Publishing

www.chemelectrochem.org

Mechanisms of Oxygen Reactions in Lithium–Air Batteries

Andrea P. Gualdron-Plata, Vivian Y. Brizola, and Vitor L. Martins*

The complicated O_2 reactions at the battery's positive electrode hinder the development of Li–air and Li–O_2 batteries. The oxygen reduction reaction (during battery discharge) and the oxygen evolution reaction (during battery charge) are still not fully elucidated, and more than one mechanism has been proposed for each process. These mechanisms greatly depend on the electrolyte's physicochemical properties, which opens the possibility of favoring a more desired one. Nonetheless, recent findings have shown that this is not always the case. Therefore, this perspective aims to provide a brief overview of the current understanding of the most widely accepted mechanisms and discuss the impact of the most recent findings.

1. Introduction

The non-aqueous Li–O_2 batteries have attracted attention due to their relatively simple structure involving freely available oxygen as an active positive electrode component.[1] A non-aqueous Li–O_2 cell consists of a porous O_2 diffusion positive electrode, metallic lithium as a negative electrode, and a non-aqueous electrolyte between them. While lithium oxidizes to Li^+, which subsequently migrates toward the positive electrode guided by an electric field, oxygen is reduced to peroxide forming Li_2O_2 Equation (1).[2,3]

$$2Li + O_2 \leftrightarrow Li_2O_2 (E = 2.96\,\text{vs}\,Li/Li^+) \quad (1)$$

Based on the discharge product capacity, Li_2O_2, these cells have a theoretical capacity of 1168 mA h g^{-1}, with a standard potential of 2.96 V and a specific energy density of 3445 W h L^{-1}.[1,4] However, attaining this theoretical value in practical applications remains a significant challenge due to parasitic reactions and the inherent instability of the battery system.[1,5] Although the overall reaction looks straightforward, the redox process is complex because of the oxygen reduction reaction (ORR) and oxygen evolution reaction (OER) on the surface of the positive electrode.

Many studies are related to the complexity of understanding the mechanisms of ORR and OER and their sluggish kinetics.[6–9] Using non-aqueous electrolytes is constantly linked to side reactions, resulting in byproducts that may promote pore clogging and fast capacity fading.[10,11] Moreover, many challenges and improvements in energy density efficiency, cyclability, and capacity still need to be studied. Recent research has explored a range of advanced methodologies to rectify these issues, mainly focusing on soluble redox mediators (RMs). These RMs act as electron–hole carriers, enabling the direct transfer of electrons between electroactive species (O_2 and Li_2O_2) and the electrode. This approach reduces the likelihood of secondary reactions, offering improved efficiency and cost-effectiveness compared to solid catalysts. Nevertheless, the inherently soluble characteristics of RMs are primarily responsible for the "shuttle effect," which entails the unrestricted movement of RMs toward the lithium (Li) negative electrode. This process can lead to electrode corrosion, resulting in structural damage, the generation of harmful byproducts, and the degradation of the RMs.[12]

This perspective offers a focused analysis of recent advancements in the fundamental understanding of mechanisms related to Li–O_2 batteries. It emphasizes the role of redox mediators, catalysts, additives, innovative techniques, and the operational conditions associated with these approaches that are currently contributing to improving Li–O_2 battery performance.

2. ORR Mechanisms

During battery discharge, the ORR takes place on the positive electrode, and there are two proposed mechanisms for the Li_2O_2 formation: surface adsorbed $LiO_{2(ads)}$ mechanism[6,7,13] or soluble $LiO_{2(sol)}$ mechanism in solution.[3,8,14,15] Nonetheless, first, the molecular oxygen O_2 taps an electron in the surface-active sites of the electrode to form a superoxide ion Equation (2).

$$O_2 + e^- \rightarrow O_2^- \quad (2)$$

After that, it is believed that one of the two mechanisms can take place, depending on many electrode and electrolyte properties. We will see later that this is still an open question for debate.

2.1. Surface Mechanism

In the surface mechanism, the superoxide ion reacts with lithium ions to form $LiO_{2(ads)}$ Equation (3), which leads to the direct

A. P. Gualdron-Plata, V. Y. Brizola, V. L. Martins
Departamento de Química Fundamental
Instituto de Química
Universidade de São Paulo
Av. Prof. Lineu Prestes 748, São Paulo, SP CEP 05508-000, Brazil
E-mail: martinsv@usp.br

A. P. Gualdron-Plata
Departamento de Engenharia Metalúrgica e de Materiais
Universidade de São Paulo
Av. Professor Mello Moraes 2463, São Paulo, SP CEP 05508-030, Brazil

© 2025 The Author(s). ChemElectroChem published by Wiley-VCH GmbH. This is an open access article under the terms of the Creative Commons Attribution License, which permits use, distribution and reproduction in any medium, provided the original work is properly cited.

© 2025 The Author(s). ChemElectroChem published by Wiley-VCH GmbH

formation of solid LiO_2 on the electrode surface. Subsequently, there are two pathways: a) two LiO_2 molecules combine to produce Li_2O_2 on the electrode surface, releasing molecular oxygen (O_2) as a byproduct in a disproportionation step that does not involve electron transfer Equation (4), forming a Li_2O_2 film, and b) a direct reduction of $LiO_{2(ads)}$ can also occur, in this case involving an electron transfer, leading to the formation of Li_2O_2 Equation (5).[2,3,7,13,16–18] Note that both surface pathways involve two electron transfers since Equation (4) needs two superoxide molecules for disproportionation.

$$O_{2(ads)} + e^- + Li^+ \leftrightarrow LiO_{2(ads)} \quad (3)$$

$$2LiO_{2(ads)} \rightarrow Li_2O_{2(ads)} + O_2 \quad (4)$$

$$LiO_{2(ads)} + e^- + Li^+ \rightarrow Li_2O_{2(ads)} \quad (5)$$

2.2. Solution Mechanism

On the other hand, in the solution mechanism, through a one-electron transfer process, O_2 is reduced to O_2^- Equation (6), which is readily solubilized in solution. Subsequently, $O_2^-{}_{(sol)}$ reacts with Li^+ Equation (7) to form superoxide $LiO_{2(sol)}$. Then, $LiO_{2(sol)}$ undergoes disproportionation as a competing reaction to form Li_2O_2 and O_2 gas or singlet oxygen in the solution Equation (8).[2,3,17,19,20]

$$O_2 + e^- \rightarrow O_{2(sol)}^- \quad (6)$$

$$O_{2(sol)}^- + Li^+ \rightarrow LiO_{2(sol)} \quad (7)$$

$$2LiO_{2(sol)} \rightarrow Li_2O_{2(sol)} + {}^3O_2/{}^1O_2 \quad (8)$$

2.3. Surface Versus Solution Mechanisms

The primary difference between these two mechanisms lies in the behavior of the superoxide (LiO_2) intermediate. To understand these mechanisms, the Pearson hard–soft acid-base (HSAB) theory is often employed, as it explains the interactions between cations and anions with the solvent, which ultimately dictate the dominant mechanism.[21] In this context, solvents are evaluated by their donor number (DN), a measure of their ability to solvate other species. A solvent with a high DN can strongly solvate other species, which, in this case, promotes the dissolution of LiO_2 into the electrolyte, which favors the solution mechanism, where Li_2O_2 grows as toroid-shaped Li_2O_2 particles.[22] Such particles do not directly block the electrode surface, allowing for higher discharge capacity, increased rates, and sustained discharge performance.[23] This process helps prevent premature battery failure by minimizing electrode passivation, making the solution mechanism the preferred route.[3,24,25] However, it faces significant challenges due to the high reactivity of the intermediates, which can attack the electrolyte solvents, leading to the generation of undesired byproducts that shorten the battery's lifespan, increase charging overpotentials, and create additional side reactions, especially under conditions of high LiO_2 solubility.[9,13,24] Conversely, a solvent with a low donor number has a weak solvating ability, which hinders the dissolution of LiO_2, promoting the surface mechanism, where Li_2O_2 forms a thin film directly on the electrode. The insulating nature of this film leads to electrode passivation, resulting in lower capacities, reduced rates, and early cell failure.[25,26] These morphological differences further highlight the critical role of solvent properties in dictating the electrochemical behavior and performance of Li–O_2 batteries.[3,25,27] Essentially, high DN solvent presents lower electrochemical stability than low DN solvent. The reason for the high DN solvent presenting a higher Li^+ solvation power is directly linked to its lower potential to be oxidized during battery charging. Additionally, side reaction products have been reported, for instance, the formation of LiOH Equation (9), which can be related to the presence of H_2O in the electrolyte[16,28–30], Li_2CO_3 Equation (10), and Li_2O Equation (11),[31] as a consequence of the carbon electrode degradation.[32] The equations of the possible side reactions are as follows[33]

$$2Li + H_2O \rightarrow 2LiOH + H_2 \quad (9)$$

$$Li_2O_2 + C + 1/2O_2 \rightarrow Li_2CO_3 \quad (10)$$

$$2Li_2O_2 + C \rightarrow Li_2O + Li_2CO_3 \quad (11)$$

2.4. Recent Developments on ORR

Understanding the mechanism increases the possibility of developing new materials, catalysts, electrolytes, and technologies. Thus, different components of the Li–O_2 battery and their impact on its performance have been thoroughly investigated in the last few years.[1] One of the strategies applied is related to promoting the mechanism in the solution pathway to achieve high capacities.[13] Xiong et al.[34] proposed a hydrogen bond-based approach to optimize solution-mediate discharge, significantly altering the reaction pathways presented in Equation (3–8). It demonstrated using 2,5-di-tert-butylhydroquinone (DBHQ) as a soluble catalyst, stabilizing the reactive oxygen species such as O_2^-, LiO_2, and Li_2O_2 through hydrogen bonding (O—H···O). This process promoted discharge via the solution mechanism by enhancing the solubility of O_2^- and Li_2O_2, generating disproportionation reactions over the formation of passivating films on the positive electrode and was compared with different additives such as 2,5-di-tert-butyl-1,4-benzoquinone (DBBQ), anthraquinone (AQ), phenol (PhOH), and H_2O that are widely used. **Figure 1**a presents the first discharge cycle of a Li–O_2 battery at different currents using the DBHQ additive, compared to DBBQ (Figure 1b) and the typical electrolyte without additives (Figure 1c). They demonstrated that DBHQ significantly enhances discharge capacity, achieving 18,945 mA h g^{-1}, compared to 4278 mA h g^{-1} with the additive-free electrolyte. Meanwhile, DBBQ, which also improves performance, reached a capacity of 13,111 mA h g^{-1}, but DBHQ remains the superior additive in terms of discharge capacity. In addition, Figure 1d–f shows a scanning electrode microscopy (SEM) and confirms the solution-phase discharge promoted by DBHQ and DBBQ. Batteries with DBBQ or no additive show small toroidal (≈500 nm) and flake-like discharge products (Figure 1e,f).

© 2025 The Author(s). ChemElectroChem published by Wiley-VCH GmbH

21960216, 2025, 12, Downloaded from https://chemistry-europe.onlinelibrary.wiley.com/doi/10.1002/celc.202500051 by University Of Sao Paulo - Brazil, Wiley Online Library on [24/06/2025]. See the Terms and Conditions (https://onlinelibrary.wiley.com/terms-and-conditions) on Wiley Online Library for rules of use; OA articles are governed by the applicable Creative Commons License

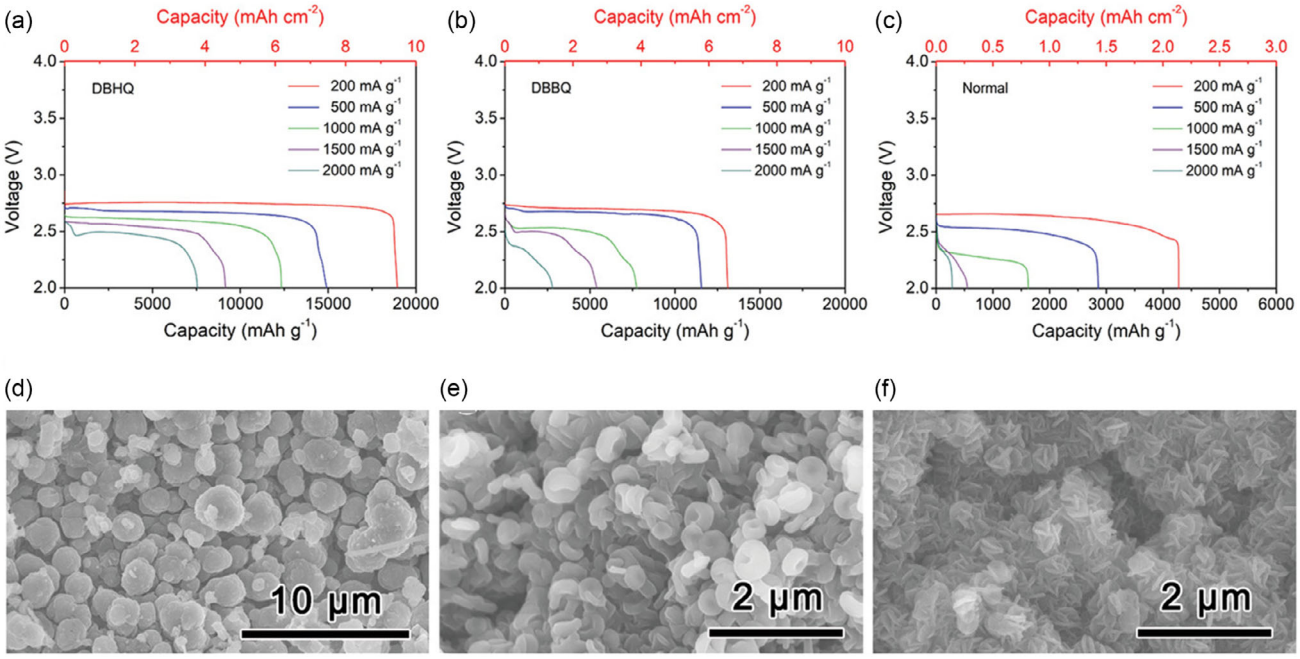

Figure 1. a–c) Deep discharge at different current rates of the Li–O_2 batteries with 1 M $LiCF_3SO_3$–TEGDME electrolyte with a) DBHQ, b) DBBQ, and c) without additive. e,f) SEM images of the discharge positive electrodes with 50 mM of d) DBHQ, e) DBBQ, and f) without additive at 200 mA g^{-1}. Adapted with permission.[34] Copyright, Wiley.

In contrast, DBHQ leads to larger toroidal structures (2–3 μm) (Figure 1d). They dissolved KO_2 in electrolytes with different concentrations of DBHQ and, using electron paramagnetic resonance (EPR), detected the unpaired electron of O_2^- demonstrating higher DBHQ concentrations increased the solubility of KO_2 and Li_2O_2, favoring the solution discharge pathway. The superior ORR performance with DBHQ was attributed to the hydrogen bond-assisted solution discharge pathway in Li–O_2 batteries.[34]

On the other hand, the solution-mediated mechanism could generate issues during the discharge. Parasitic reactions between superoxide/peroxide species and electrolytes produce byproducts on oxygen-evolving interfaces, developing problems with the charge potential and poor cyclability.[35] Zhao et al.[36] used in situ surface-enhanced Raman spectroscopy, density functional theory (DFT) calculations, and differential electrochemical mass spectroscopy (DEMS) to provide direct evidence of intermediates in the ORR in Li–O_2 batteries. A model anthraquinone gold (Au–AQ) electrode was employed to study the solution-mediated ORR mechanism. They proposed a reaction mechanism in which AQ is first reduced to LiAQ, then reacts with O_2, forming $LiAQO_2$, and finally decomposes to release LiO_2, which disproportionates to form Li_2O_2, providing a valid mechanism to regulate discharge product.

Zhao et al.[37] investigated the fundamental role of Lewis basic sites in the chemistry of Li–O_2 batteries, an area that has been little explored until now. They designed an electrocatalyst based on a metal-organic framework denoted UIO-66-NH_2, which contains Lewis basic sites to analyze the impact on the kinetics and growth of Li_2O_2. DFT calculations revealed that the Lewis basic sites act as electron donors, favoring the activation of O_2 and Li_2O_2, which reduces the charge and discharge potential. Furthermore, in situ Fourier transform infrared spectroscopy (FTIR) spectra and DFT results demonstrate that these sites shift the Li_2O_2 growth mechanism from surface adsorption to solution-mediated growth by capturing Li^+ during the discharge process. The design of novel electrocatalysts with dual acid-base centers could improve reaction kinetics.

Zheng et al.[38] fabricated a $CoSe_2$-based electrocatalyst on Ti_3C_2 MXene as an oxygen electrode for Li–O_2 batteries, studying the influence of enhanced interfacial electronic interaction caused by cation vacancies in the electrode on the kinetics of the reaction (OER/ORR). Using experimental characterization and DFT calculations, they demonstrated that the Co–C–Ti electron transfer, promoted by Co cation vacancies, facilitates electron transfer from Ti_3 Ti_3C_2 MXene to $CoSe_2$, optimizing the adsorption of reactants and intermediates while reducing the kinetic barrier, resulting in an overpotential of 0.35 V, a capacity of 12,738.6 mA h g^{-1} and stability over 250 cycles at 500 mA g^{-1}. Xu et al.[39] designed an electrode catalyst with vanadium pentoxide, containing abundant vanadium vacancies on V_2C MXene, which showed low overpotential, high energy efficiency (83.4%), and excellent cycling stability (501 cycles) with a limited capacity by 1000 mA h g^{-1}. The vanadium vacancies provide active sites, enhancing catalytic performance by increasing the adsorption energies of Li_2O_2 and LiO_2 intermediates. Du et al.[40] fabricated Sr and Fe co-doped $LaCoO_3$ (LSCFO) porous nanoparticles for Li–O_2 batteries. LSCFO-based batteries exhibited high discharge capacities (26,833 mA h g^{-1}), low overpotentials (0.32 V), and good cycling stability (200 cycles at 300 mA g^{-1}). These results are attributed to the large surface area and mesoporous structure. Calculations revealed that Sr and Fe co-doping enhanced Co 3d−O 2p covalency, reducing LiO_2 intermediate adsorption energy and

© 2025 The Author(s). ChemElectroChem published by Wiley-VCH GmbH

21960216, 2025, 12, Downloaded from https://chemistry-europe.onlinelibrary.wiley.com/doi/10.1002/celc.202500051 by University Of Sao Paulo - Brazil, Wiley Online Library on [24/06/2025]. See the Terms and Conditions (https://onlinelibrary.wiley.com/terms-and-conditions) on Wiley Online Library for rules of use; OA articles are governed by the applicable Creative Commons License

promoting efficient Li_2O_2 decomposition. The new electrocatalyst offers a strategy for improving the performance of Li–O_2 batteries.

Zhu et al.[35] demonstrate that the solvent DN directly influences the capacity and stability of Li–O_2 batteries. **Figure 2**a,b compares electrolytes prepared with the solvents TEGDME (G4, DN= 17) and DMSO (DN= 29.8). Using a MnO_2 positive electrode with nanoflakes structure, charge and discharge cycles were performed, showing that in an electrolyte containing 100% TEGDME, the battery reached 144 cycles. In comparison, in 100% DMSO, cyclability was reduced to 37 cycles. However, as shown in **Figure 3**c, DMSO provided a higher discharge capacity (2.54 mA h cm^{-2}) compared to TEGDME (0.73 mA h cm^{-2}), along with binary mixtures ratio (20:80, 50:50, and 80:20 DMSO:TEGDME). It is shown that, despite its low stability, DMSO (high DN= 29.8) allows a higher loading capacity compared to TEGDME (low DN= 17), which, although having a lower loading capacity, offers higher cyclic stability, and mixing the solvents offers an improvement in the cell performance. Electrochemical impedance spectroscopy (EIS) showed that resistance increases more rapidly during discharge in TEGDME, attributed to the formation of Li_2O_2 in film growth (surface mechanism), which blocks the positive electrode and reduces capacity. In contrast, in DMSO, Li_2O_2 deposits in a toroidal shape (solution mechanism), reducing interfacial resistance and promoting higher charge capacity but with lower stability.

It is essential to recognize that the design of these cells, in conjunction with emerging technologies such as simulation, is advancing research on these batteries.[41] For example, Li et al.[19] developed an advanced 1D model using a finite element method

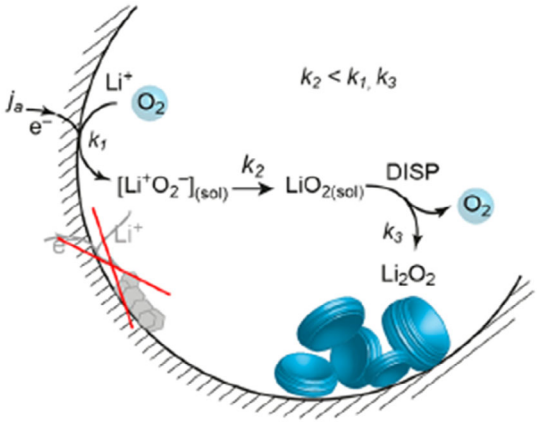

Figure 3. Illustration of the sketch of oxygen reduction and Li_2O_2 formation mechanism and morphology. Reprinted with permission.[9] Copyright 2022, American Chemical Society.

that considers the discontinuous deposition of Li_2O_2 and the formation of Li_2CO_3 due to electrolyte degradation. This dual consideration makes it unique compared to previous models. This model analyzed positive electrode properties such as porosity, thickness, current density, and electrolyte parameters such as oxygen solubility and diffusivity that affect capacity and energy density. It found that increasing porosity and improving oxygen transport optimize performance, but byproduct accumulation reduces cyclability.

Additionally, they evaluated current density, a key parameter in battery performance. The results showed a specific capacity of

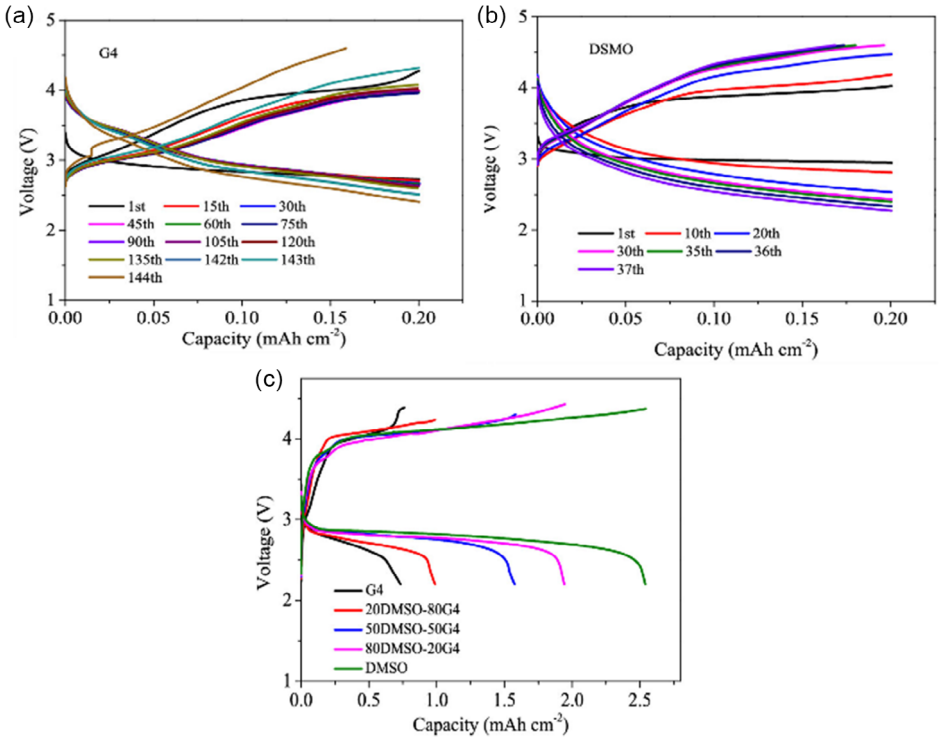

Figure 2. Cell potential profiles of Li–O_2 batteries in a) TEGDME and b) DMSO during the cycling at 0.05 mA cm^{-2} with a limited capacity of 0.20 mA h cm^{-2}. a) DMSO, b) TEGDME, and c) voltage profiles of Li–O_2 batteries in electrolytes with TEGDME (G4), DMSO, and DMSO–G4(TEGDME) binary solvents. Reprinted with permission.[84] Copyright 2022, American Chemical Society.

© 2025 The Author(s). ChemElectroChem published by Wiley-VCH GmbH

21960216, 2025, 12, Downloaded from https://chemistry-europe.onlinelibrary.wiley.com/doi/10.1002/celc.202500051 by University Of Sao Paulo - Brazil, Wiley Online Library on [24/06/2025]. See the Terms and Conditions (https://onlinelibrary.wiley.com/terms-and-conditions) on Wiley Online Library for rules of use; OA articles are governed by the applicable Creative Commons License

269.9 mA h g^{-1}_{carbon} to 1354.9 mA h g^{-1}_{carbon} when the current density increased from 0.05 to 0.5 mA cm^{-2}.[19] These values are comparable to those reported experimentally by Read,[42] who studied the effect of the electrolyte on discharge capacity at different density currents, suggesting consistency in the observed trend. However, it is essential to note that direct experimental validation under the simulated conditions was not performed. The simulations are limited by ideal scenarios, considering only one redox reaction associated with Li_2CO_3. At the same time, previous studies have demonstrated the presence of more complex parallel reactions due to the interaction of the solvent, salts, and other products.[33] Although they have limitations, simulations are a valuable tool for exploring different scenarios and isolating key parameters, which can contribute to reducing the time required to perform multiple experimental trials.

Finding a stable electrolyte with high oxygen solubility and low volatility or reducing the overpotential to improve the round-trip efficiency is necessary for enhancing performance.[37] Prehal et al.[9] provide evidence that Li_2O_2 forms across a wide range of electrolytes, carbons, and current densities as particles via solution-mediated LiO_2 disproportionation, finding contradicts the widely accepted model that weakly solvating electrolytes lead to surface film growth, while strongly solvating electrolytes favor large toroidal particles. They used rotating ring-disk electrode (RRDE) measurements and SEM to demonstrate the presence of soluble LiO_2, even in weakly solvating electrolytes. Determining particle morphology and achievable capacities is crucial to describe a unified O_2 reduction mechanism, which can explain all found capacity relations and Li_2O_2 morphologies with exclusive solution discharge. Figure 3 shows a scheme of the mechanism and morphology obtained in experiments.

In summary, for the ORR, two widely accepted mechanisms (via surface or solution) could be chosen at first, especially on the electrolyte's solvent DN. Nonetheless, the recent discoveries highlighted above show that solvents with low DN can solubilize Li_2O and induce the solution mechanism when not expected, achieving high capacities believed to be possible only in high DN solvents. These recent findings open opportunities for novel electrolyte design and explore low DN solvents in electrolytes with higher electrochemical stability. Moreover, these findings can also impact studies involving OER, as discussed in the following section.

3. OER Mechanisms

Despite being poorly elucidated, the charge reaction mechanisms have been widely discussed and are a decisive factor in understanding and overcoming the main challenges associated with the operation of Li–O_2 batteries[3,43–46]. Thus far, two widely accepted proposals exist: 1) a one-step oxidation mechanism, determined by gravimetric analyses performed by Ogasawara et al.[47] in which Li_2O_2 particles are completely dissociated into Li^+ and O_2 through a process involving a direct transfer of two electrons (Equation (12))

$$Li_2O_2 \rightarrow 2Li^+ + 2e^- + O_2 \quad (12)$$

and (2) a two-step mechanism initially established by Lu and Shao–Horn,[48] based on an experimental study using the galvanostatic intermittent titration technique (GITT) and potentiostatic intermittent titration technique (PITT) that is based on the partial removal of Li^+ ions from the peroxide (as in a delithiation step). Kinetic studies, together with appropriate characterizations, allowed the identification of a two-step mechanism, which are:[3,47,49] 2a) topotactic delithiation, characterized by a slope region with low overpotentials (< 400 mV), in which Li^+ is removed from the outer part of Li_2O_2 particle to form a nonstoichiometric lithium-deficient peroxide, $Li_{2-x}O_2$, keeping the solid structure and its orientations Equation (13).

$$Li_2O_2 \rightarrow Li_{2-x}O_2 + xLi^+ + xe^- \quad (13)$$

The complete delithiation process via a solid-solution might also generate superoxide species (LiO_2) Equation (14), which can be disproportionated to evolve O_2 and produce Li_2O_2 (Equation (15)) in an overall two-electron transfer per O_2 OER process (Equation (16)). This mechanism proposes that the LiO_2-like species are produced by the delithiation process of a nonstoichiometric lithium-deficient species.[16,19,48,50,51]

$$Li_{2-x}O_2 \rightarrow LiO_2 + (1-x)Li^+ + (1-x)e^- \quad (14)$$

$$2LiO_2 \rightarrow Li_2O_2 + O_2 \quad (15)$$

$$Li_2O_2 \rightarrow 2Li^+ + 2e^- + O_2 \quad (16)$$

The topotactic delithiation mechanism (2a) was also evaluated by theoretical investigation, where Kang et al.[49] used ab initio calculations to explain this process. In their model, localized oxidation of Li_2O_2 promotes the removal of one antibonding electron from Li_2O_2, resulting in the formation of nonstoichiometric $Li_{2-x}O_2$ products. These products maintain a peroxide ion structure (O_2^{2-}) but with a shorter bond length. The reduction in bond length makes the peroxide ion structure (O_2^{2-}) comparable to that of transition metals oxides, leading to a behavior similar to what is observed in lithium intercalation mechanisms, which leads some groups to name this process as deintercalation mechanism.[49] The second is 2b) nucleation and growth, characterized by the bulk oxidation of Li_2O_2 particles, producing Li^+ and O_2 through a two-phase transition step (Equation (17)). Supercritical nuclei (such as Li and O vacancies) are formed.[48,52,53] Then, the growth of the formed nuclei in both quantity and size is observed, which leads to an increase in the active electrochemical area for reaction kinetics.[48,52,54]

$$Li_2O_2 \rightarrow 2Li^+ + 2e^- + O_2 \quad (17)$$

Ganapathy et al.[55] investigated these mechanism steps throughout operando X-ray diffraction patterns collected on Li–O_2 cells for a complete charge cycle (Figure 5a). The disappearance of peaks (1 0 0) and (1 0 1) through time proved that the Li_2O_2 was removed during the charge (Figure 5b). The authors used Rietveld refinement of diffraction data. They identified a peak broadening in both peaks during the charge and plotted it as a function of charge capacity (Figure 5c). This result indicated

© 2025 The Author(s). ChemElectroChem published by Wiley-VCH GmbH

21960216, 2025, 12, Downloaded from https://chemistry-europe.onlinelibrary.wiley.com/doi/10.1002/celc.202500051 by University Of Sao Paulo - Brazil, Wiley Online Library on [24/06/2025]. See the Terms and Conditions (https://onlinelibrary.wiley.com/terms-and-conditions) on Wiley Online Library for rules of use; OA articles are governed by the applicable Creative Commons License

an increase in average crystallite size. The authors also obtained SEM images at different states of charge (Figure 5d) and observed an isotropic crystalline platelet shape toward the end of charge. This behavior aligns with the proposal that the smallest crystals initially decompose and suggests a slight change in the average particle shape at the end of charging, where the particles become more isotropic, indicating that thinner platelet crystallites are oxidized first in a plate-by-plate-like oxidation. Also, the Li-occupancy parameters indicate that some Li vacancies were created, resulting in a small fraction of nonstoichiometric $Li_{2-x}O_2$. At the same time, a nonlinear decrease in peak intensity was detected during charge, coinciding with a voltage increase starting at 3.4 V and then declining linearly across the second plateau until reaching ≈3.9 V (**Figure 4**a,b). A practically constant behavior under the integrated area of the reflections indicated a preferential decomposition of surface LiO_2 species and/or any amorphous Li_2O_2 component present in the lower voltage regime (2.8–3.4 V), which is in line with the idea of Li_2O_2 being first oxidized in the electrode/particle contact. In the higher voltage regime (3.4–3.9 V), the second plateau is characterized by a linear decrease in integrated area under the reflections, indicating the complete oxidation of Li_2O_2 grains and the evolution of O_2. These results, combined with a gradual reduction of the Li-occupancy observed during the charge (**Figure 5**e) from ≈3.2 V, corroborate the proposed mechanism via nonstoichiometric lithium-deficient species intermediates. The two oxidation stages were correlated to a charging curve for a better understanding (Figure 5a).[55]

Another possible mechanism is the direct formation of the intermediate lithium superoxide (LiO_2) due to its higher conductivity and better charge transport properties than Li_2O_2, which could moderate the electrical transport losses.[56] Lu and Shao–Horn[48] theorized a "deintercalation process" via a solid-solution route that would generate a LiO_2 directly from Li_2O_2 without the formation of a nonstoichiometric $Li_{2-x}O_2$ under low potentials (< 400 mV), as shown on Equation (18).

$$Li_2O_2 \rightarrow LiO_2 + Li^+ + 2e^- \quad (18)$$

Stabilizing LiO_2 has been sought in some works to minimize charging overpotentials and enhance charge transport, aiming to develop more efficient devices. Graphene oxides (GO) have stood out, serving as effective catalysts for the OER due to their abundance of oxygen-containing functional groups (carboxyl, hydroxyl, and epoxy), which act as catalytic active centers. These properties help reduce charging overpotential and enhance battery cycling performance.[56–58]

Cai et al.[57] investigated the GO adsorption mechanism of action through the Vienna ab initio Simulation Package. According to their findings, the adsorption properties of Li_2O_2 or LiO_2 molecules on GO enhance as the oxidation degree of GO increases. Computational results suggested that an increase in the oxidation degree of graphene may lead to a gradual shortening of O–O bond lengths and lengthening of Li–O bond lengths enhance the charge transfer from L_2O_2 or LiO_2 molecules to GO. Recently, Yu et al.[59] proposed a carbon positive electrode design based on a hierarchical porous membrane based on graphene mesosponge (GMS) integrated into a binder-free sheet, denoted GMS sheet. The structure GMS sheets scales were controlled, aiming to provide more active sites to favor 1) the mass transfer of Li^+ and the nucleation of intermediates (LiO_2) through micro/mesopores and 2) the mass transfer of O_2 and, consequently, the growth of discharge products through macropores. The galvanostatic full-discharge–charge curves indicated that an

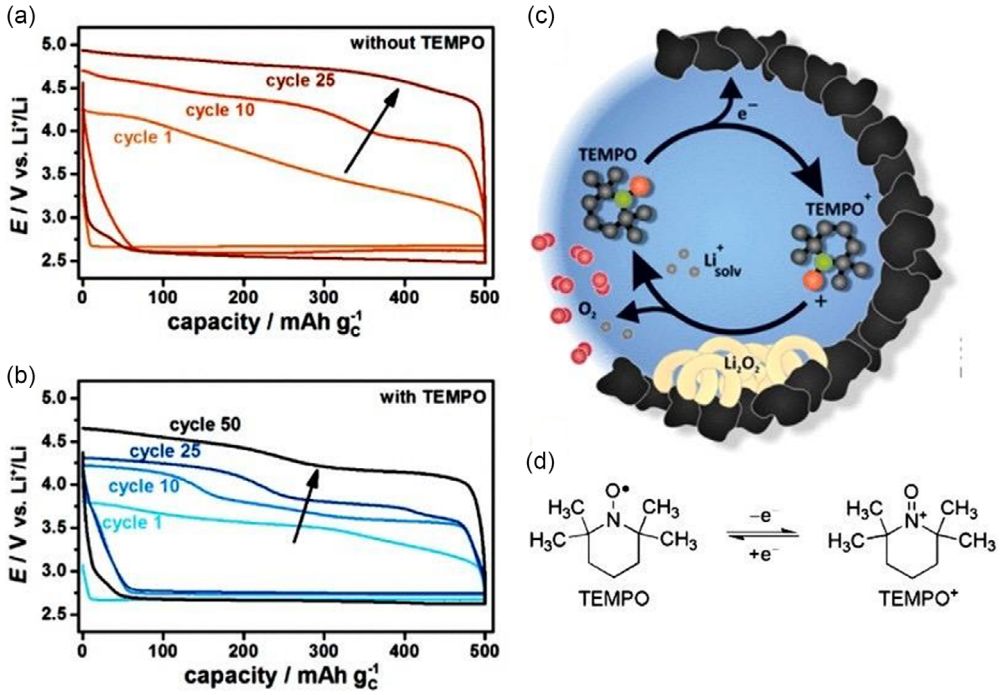

Figure 4. a) Cycling stability of Li–O_2 cell without TEMPO; b) cycling stability of Li–O_2 cell with TEMPO; c) mechanism of Li_2O_2 oxidation illustration in the presence of the redox mediator TEMPO; and d) mechanism of activity of TEMPO. Reprinted with permission.[60] Copyright 2014, American Chemical Society.

© 2025 The Author(s). ChemElectroChem published by Wiley-VCH GmbH

21960216, 2025, 12, Downloaded from https://chemistry-europe.onlinelibrary.wiley.com/doi/10.1002/celc.202500051 by University Of Sao Paulo - Brazil, Wiley Online Library on [24/06/2025]. See the Terms and Conditions (https://onlinelibrary.wiley.com/terms-and-conditions) on Wiley Online Library for rules of use; OA articles are governed by the applicable Creative Commons License

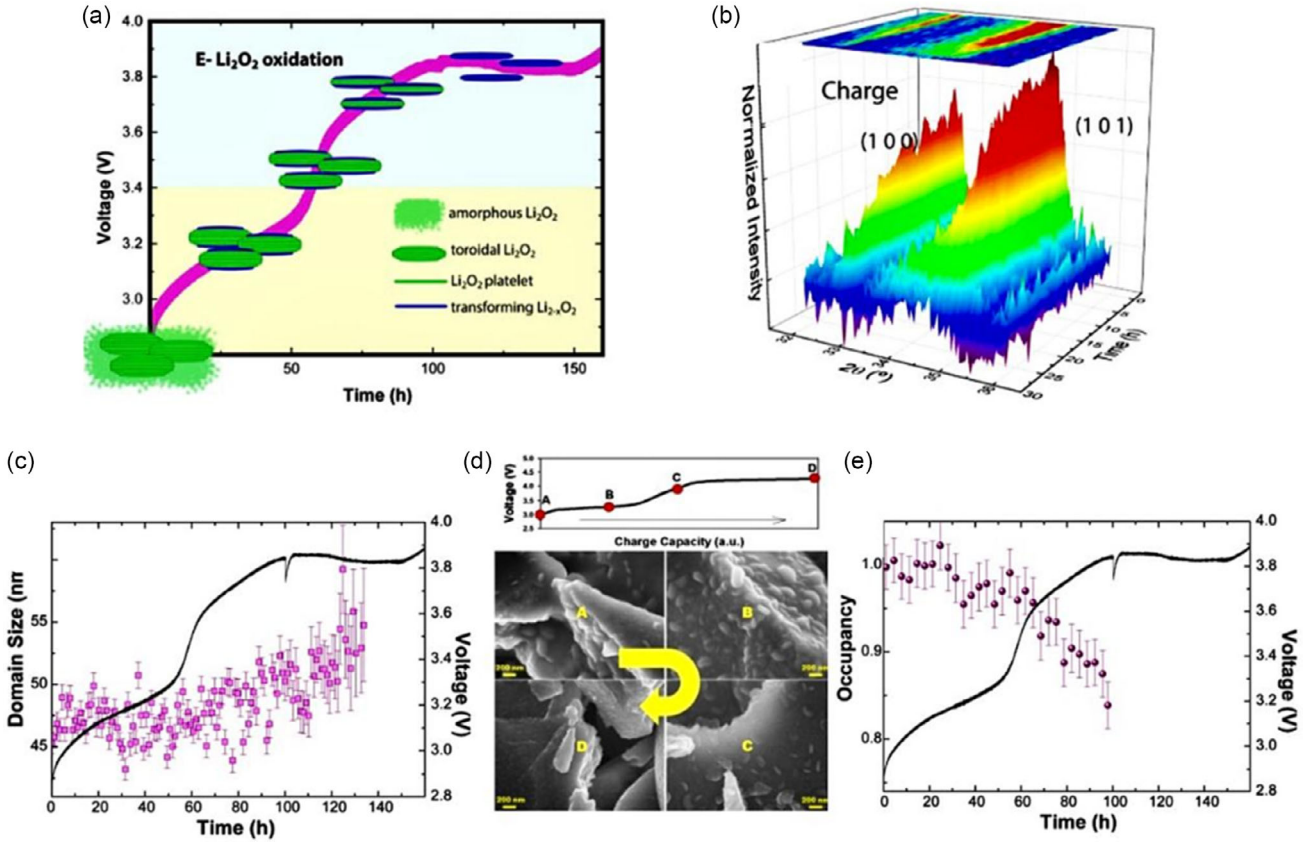

Figure 5. a) Mechanism of Li_2O_2 oxidation during the charging process as determined from operando XRD; b) 3D charge plots of the XRD patterns of the positive electrode in the 2θ region of 32°–36°, recorded operando as a function of time of charge; c) average domain size; d) SEM images recorded from electrodes at different stages of oxidation; and e) average lithium occupancy. Reprinted with permission.[55] Copyright 2014, American Chemical Society.

increase in the porosity of the GMS sheet corresponds to a reduction in the palletization force of the material, which is associated with a lower graphene stacking number. This, in turn, leads to a substantial enhancement in the gravimetric capacity of the devices, achieving values exceeding 6200 mA g^{-1} at a relatively high current density of 0.4 mA cm^{-2}, and notably, without the use of a catalyst. The analysis was performed in the presence of 2,2,6,6-tetramethylpiperidinyloxyl (TEMPO) as a redox mediator to reduce the charge potential and lithium nitrate ($LiNO_3$) as a negative electrode protector to minimize the "shuttle effect." This method improved cyclability, increasing the stable cycles from 27 to 55 (in a fixed capacity of 500 mAh g_c^{-1}), without and with TEMPO, respectively (Figure 4a,b). The system characterization by time-of-flight secondary ion mass spectrometry (TOF-SIMS), N_2 ad-/desorption isotherms, and in situ X-ray diffraction (XRD) enabled the elucidation of a possible mechanism where the charging process corresponds to a characteristic decomposition of Li_2O_2, where the RM is preferentially electrochemically oxidized to RM^+ and then chemically reacts with Li_2O_2, as already discussed in by others before, as is shown in Figure 4c,d.[60] However, the oxidation path through LiO_2 is more prone to the formation of singlet oxygen due to the disproportionation step.

Subsequently, Wang et al.[51] explored the charging mechanism with a thin film rotating ring disk electrode in the presence of electrolytes with solvents with varying degrees of DN. The study and synchrotron-based X-ray absorption near-edge structure (XANES) spectroscopy analyses demonstrated that soluble LiO_2 species are formed in high-DN solvents, promoting low cycling stability. SEM and XANES analyses in high-DN solvents (such as DMSO and N-methylimidazole) revealed that after 80% of the charge, a toroidal structure re-formed in the layer, indicating a probable disproportionation mechanism of soluble LiO_2 species, leading to the regeneration of crystalline Li_2O_2 particles. Meanwhile, charging with low-DN electrolytes (like TEGDME) revealed a gradual shrinkage of the particles until their complete disappearance at the end of the reaction. These findings led to the proposal of solvent-controlled Li_2O_2 decomposition mechanisms, as presented in Equation (19)–(21) for electrolytes with high-DN solvents and in Equation (22) and (23) for electrolytes with low-DN solvents.[51]

Using high DN solvent

$$Li_2O_2 \rightarrow Li^+ + xe^- + Li_{2-x}O_2 \quad (19)$$

$$Li_{2-x}O_2 \rightarrow (1-x)e^- + (1-x)Li^+ + LiO_2^* \quad (20)$$

$$LiO_2^* + LiO_{2(sol)} \rightarrow Li_2O_{2(s)}^* + O_2 \quad (21)$$

Using low DN solvent

$$Li_2O_2 \rightarrow Li^+ + xe^- + Li_{2-x}O_2 \quad (22)$$

© 2025 The Author(s). ChemElectroChem published by Wiley-VCH GmbH

21960216, 2025, 12, Downloaded from https://chemistry-europe.onlinelibrary.wiley.com/doi/10.1002/celc.202500051 by University Of Sao Paulo - Brazil, Wiley Online Library on [24/06/2025]. See the Terms and Conditions (https://onlinelibrary.wiley.com/terms-and-conditions) on Wiley Online Library for rules of use; OA articles are governed by the applicable Creative Commons License

$$Li_{2-x}O_2 \rightarrow (2-x)e^- + (2-x)Li^+ + O_2 \quad (23)$$

The superoxide disproportionation can also be responsible for the singlet oxygen formation ($^1O_2$), which is reactive and can be responsible for electrolyte and electrode degradation. On that matter, RMs facilitate the oxidation of Li_2O_2 and avoid $^1O_2$ formation, but existing low-voltage mediators do not provide fast charging rates.[61–63] Anh[64] reported a mechanism of Li_2O_2 oxidation by mediator redox and its influence on $^1O_2$ evolution. The study showed that the disproportionation step of LiO_2 to $^3O_2$ and peroxide ($2LiO_2 \leftrightarrow Li_2O_2 + {}^3O_2$), and not the one-electron oxidation of LiO_2 to $^1O_2$ or $^3O_2$ ($RM^+ + LiO_2 \leftrightarrow RM + {}^1O_2 + Li^+$or $RM^+ + LiO_2 \leftrightarrow RM + {}^3O_2 + Li^+$), is favorable. Moreover, they demonstrated that the yield of singlet oxygen does not correlate with degradation, suggesting that other factors contribute to battery failure: Low-voltage mediators (<3.3 V) are inefficient and too slow, and high-voltage mediators (>3.7 V) enable faster charging but result in poor round trip energy efficiency.

Also, a thin-film RRDE voltammetry analysis confirmed the soluble intermediate species (LiO_2) generated upon Li_2O_2 oxidation due to the increasing current in the ring during a first scan from open-circuit potential (OCP, ≈3.10 V vs. Li/Li^+) to 1.5 V versus Li/Li^+ in DMSO and TEGDME solution medium. In this instance, the high DN solvent (DMSO) reached a higher charging capacity than the low DN solvent (TEGDME), being 83 mA h g_c^{-1} (4.0 μA h) and 78 mA h g_c^{-1} (3.8 μA h), respectively.[51]

As mentioned, the formation of $^1O_2$ during the charging process is problematic due to its reactivity, so its production has been highly investigated through its essential role in promoting parasitic reactions.[43,65] The first hypothesis for the $^1O_2$ generation emerged from electrochemical experimental research, which employed potentiodynamic cycling with galvanostatic acceleration (PCGA) and cyclic voltammetry (CV) in a solid-state cell, using a poly(ethylene oxide)–lithium triflate (PEO-$LiCF_3SO_3$) as the solid electrolyte.[66] During the anodic scanning on PCGA and CV measurements (oxidation process) in the 2.9–3.1 V versus Li/Li^+ range, no significant current peak was identified, suggesting an intermediate state among the oxidation products. By associating the oxidation voltage of other peroxides (such as H_2O_2) together with the good reversibility of the process, the authors proposed a new mechanism where the formation of $^1O_2$ could reduce the energy barrier of the process.

The hysteresis frequently observed in Li–O_2 batteries is due to a charging overpotential, a critical factor influencing battery performance and reducing energy efficiency and electrode degradation. One potential solution to mitigate these issues is the use of RMs, as already mentioned, which facilitate electrochemical reactions during charge and discharge processes. Various RMs have been developed, including iron phthalocyanine (FePc), 2,2,6,6-tetramethylpiperidinyloxyl (TEMPO), 2,5-di-tert-butyl-1, 4-benzoquinone (DBBQ), lithium bromide (LiBr), and lithium nitrate ($LiNO_3$).[67] However, these mediators also present certain drawbacks, such as redox shuttle reactions and the deterioration of lithium metal, which can negatively impact overall battery performance. Qiao[68] designed a MOF-based separator which inhibited the permeation of RMs to the Li-anode. They show an improvement in the cyclability compared with a typical separator of Celgard, with low overpotential and superior electrochemical performance over 100 cycles (5000 mA h g^{-1}) at a current density of 1000 mA g^{-1}.[68]

More recently, it has been investigated that O_2^- is prone to generate $^1O_2$ in the presence of Li^+ (aprotic electrolyte) or the presence of H^+ (aqueous electrolytes) by the disproportionation mechanism, as demonstrated in Equation (24) and (25).[63,69]

Aprotic electrolytes

$$2O_2^- + 2Li^+ \rightarrow Li_2O_2 + {}^1O_2 \quad (24)$$

Protic electrolytes

$$2O_2^- + 2H^+ \rightarrow H_2O_2 + {}^1O_2 \quad (25)$$

With that, it has been essential to detect $^1O_2$ and to develop strategies to mitigate its formation, thereby minimizing side reactions and optimizing OER kinetics. Various approaches have been explored to enhance battery performance, focusing on 1) RM that enables fast charging rates and suppresses the generation of $^1O_2$;[64,70–72] 2) multifunctional graphene that modifies the adsorption energy of electroactive species and enhances electron transport from the positive electrode;[62,71,73–77] 3) physical quenchers that deactivate $^1O_2$, minimizing side reactions; 4) battery design modifications that improve gas flow and operational flexibility;[72] and (5) optimized cycling protocols to extend cell lifespan.[78] Wandt et al.[79] have detected the $^1O_2$ formed during the charge at potentials above 3.5 V. They used a sterically hindered secondary amine (2,2,6,6-tetramethyl-4-piperidone (4-Oxo-TEMP)) as a spin trap to form a stable and detectable radical. The trapping agent selection was highly specific, ensuring the choice of a non-reactive compound with superoxide radicals while being detectable through operando electron paramagnetic resonance spectroscopy. Along with online electrochemical mass spectrometry, four main charge stages were detected. According to the authors, Stage I was associated with oxygen evolution by the Li_2O_2 oxidation as the primary electrochemical reaction. Once the electrode potential exceeds about 3.55 V, Stage II is initiated, and the 4-Oxo-TEMPO amount starts to increase, indicating that this increase is caused by the reaction of the spin trap with $^1O_2$. Stage III displays a decrease in 4-Oxo-TEMPO concentration because of the one e^- oxidation reaction of the nitroxyl radical. At last, above ≈3.9 V, Stage IV is initiated, with another increase in the concentration of 4-Oxo-TEMPO accompanied by oxygen consumption, indicating that the spin trap was electrochemically oxidized, which prompted a reaction with triplet oxygen to form 4-Oxo-TEMPO. Besides this, several other studies have successfully detected singlet oxygen during the charging reaction of Li–O_2 batteries.[62,80,81] Jiang et al.[76] used ruthenium tris(bipyridine) cations as a soluble catalyst to capture O_2^- dimers and promote intramolecular charge transfer, thereby facilitating both discharge and charge processes by accelerating their disproportionation reaction by decreasing the reaction's energy barrier from 7.70 to 0.70 kcal mol^{-1}. This approach extended the device's lifespan by 230 cycles, maintaining a fixed capacity of 0.5 mA h cm^{-2} at 0.2 mA cm^{-2}, with a maximum capacity of 2.9 mA h cm^{-2} achieved under this current density. Simultaneously, this approach mitigates O_2^- and its associated side reactions. The use of RMs for the charging

© 2025 The Author(s). ChemElectroChem published by Wiley-VCH GmbH

21960216, 2025, 12, Downloaded from https://chemistry-europe.onlinelibrary.wiley.com/doi/10.1002/celc.202500051 by University Of Sao Paulo - Brazil, Wiley Online Library on [24/06/2025]. See the Terms and Conditions (https://onlinelibrary.wiley.com/terms-and-conditions) on Wiley Online Library for rules of use; OA articles are governed by the applicable Creative Commons License

process seems crucial to diminish (or eliminate) the formation of $^1O_2$ and avoid the large overpotential. Moreover, the RM may accelerate the electrochemical kinetics involved in Li_2O_2 oxidation process and steer the oxidation to the particle/electrolyte interface instead of the particle/electrode interface.

In conclusion, many fundamental works may have been recently published to better describe ORR and OER in Li–O_2 batteries, showing that understanding and controlling the potential mechanisms are pivotal for such technology to thrive. At this point, it is clear that new electrolyte designs could help to select the ORR solution mechanism to achieve higher capacities even with low DN solvent, which usually has expanded electrochemical stability, which in turn will be beneficial in avoiding electrolyte decomposition on battery charging. On the other hand, the use of RM must also be considered to achieve faster kinetics on OER and suppress the formation of $^1O_2$ while consistently considering the necessity of employing a protective agent to mitigate the "shuttle effect." These recent fundamental findings clearly show the importance of using in situ and operando techniques to fully describe the mechanisms of Li–O_2 operation for a complete description of newly employed materials.

A critical bottleneck related to ORR and OER is the charge–discharge hysteresis, as already mentioned in this perspective. Nonetheless, recent approaches focus on tackling this issue by reducing the overpotential of both oxygen reactions, bringing them closer to the thermodynamic value. One interesting approach is the use of photomediated electrocatalysts present in the positive electrode.[82,83] Lv et al.[82] produced an electrocatalyst based on cobalt-tetramino-benzoquinone, which, under visible light illumination, reduces the overpotential of both reactions and obtained an energy round trip efficiency of 94%. The illuminated photoelectrocatalyst favors the formation of LiO_2 during reduction, which will be further reduced to peroxide in a 3.1 V versus Li/Li^+. Co plays an essential role in this reaction's mechanism, and the authors showed its importance through DFT calculation and experimental testing. Moreover, the photoelectrocatalyst is also active during the charging process, forming pairs of electrons/holes and favoring the oxidation process. More recently, Wen et al.[83] also reported a light-intermediated Li–O_2 battery. They used a MOF based on Fe and Ni that together induce the formation of radical $^{\bullet}O_2^-$, that combine with Li^+ to form a high concentration of LiO_2 near the electrode surface, and that then is further reduced or disproportionates to peroxide, similar to the previous example, forming an amorphous film. The holes generated in the photoelectrocatalyst by light also improve the OER, reducing its overpotential. The overall process presents an overpotential of 280 mV and an energy round trip efficiency of 92%.

The Li–O_2 battery has incredible potential due to its high capacity and energy density, but the many obstacles to be overcome make realizing this technology a long-term expectation. Despite these hurdles, recent advancements, as highlighted in this perspective, demonstrate the crucial role of fundamental studies in addressing key issues and guiding practical improvements. Developing novel electrolytes is one of the most critical aspects in achieving stable cycling and extended cycle life. Historically, solvents with high DN have been preferred due to their ability to dissolve LiO_2, leading to higher discharge capacities. However, a significant drawback of these high DN solvents is their narrow electrochemical stability window, which makes them prone to decomposition and side reactions during cycling. The findings discussed in this perspective reveal an alternative pathway—achieving high discharge capacity using low DN solvents. This discovery challenges conventional wisdom and suggests that low DN solvents may offer a route to achieving both high capacity and long cycle life. These insights open new possibilities for designing electrolyte formulations that balance capacity and stability, potentially bringing Li–O_2 batteries closer to commercial viability. Beyond electrolyte innovation, integrating advanced electrocatalysts, RMs, and even photo-assisted catalytic strategies will be crucial in further refining Li-O_2 battery performance. Developing highly efficient (photo) electrocatalysts can lower overpotentials, reduce charge–discharge hysteresis, and enhance reaction kinetics, making the system more energy-efficient. Combined with an optimized electrolyte formulation, these advancements could lead to a next-generation Li–O_2 battery with improved longevity, efficiency, and practicality for real-world applications.

Acknowledgements

A.P.G.-P. and V.Y.B. contributed equally to this work. The authors acknowledge FAPESP for funding: 2019/26309-4, 2024/17269-7, and 2024/01204-3.

Conflict of Interest

The authors declared no conflict of interest.

Data Availability Statement

The data that support the findings of this study are available from the corresponding author upon reasonable request.

Keywords: lithium–air battery · lithium–O_2 battery · oxygen evolution reaction · oxygen reduction reaction

[1] A. C. Luntz, B. D. McCloskey, *Chem. Rev.* **2014**, *114*, 11721.
[2] Z. Lyu, Y. Zhou, W. Dai, X. Cui, M. Lai, L. Wang, F. Huo, W. Huang, Z. Hu, W. Chen, *Chem. Soc. Rev.* **2017**, *46*, 6046.
[3] D. Aurbach, B. D. McCloskey, L. F. Nazar, P. G. Bruce, *Nat. Energy* **2016**, *1*, 1.
[4] D. G. Kwabi, N. Ortiz-Vitoriano, S. A. Freunberger, Y. Chen, N. Imanishi, P. G. Bruce, Y. Shao-Horn, *MRS Bull.* **2014**, *39*, 443.
[5] T. Liu, J. P. Vivek, E. W. Zhao, J. Lei, N. Garcia-Araez, C. P. Grey, *Chem. Rev.* **2020**, *120*, 6558.
[6] B. D. McCloskey, R. Scheffler, A. Speidel, G. Girishkumar, A. C. Luntz, *J. Phys. Chem. C* **2012**, *116*, 23897.
[7] V. Viswanathan, J. K. Nørskov, A. Speidel, R. Scheffler, S. Gowda, A. C. Luntz, *J. Phys. Chem. Lett.* **2013**, *4*, 556.
[8] C. O. Laoire, S. Mukerjee, K. M. Abraham, E. J. Plichta, M. A. Hendrickson, *J. Phys. Chem. C* **2010**, *114*, 9178.
[9] C. Prehal, S. Mondal, L. Lovicar, S. A. Freunberger, *ACS Energy Lett.* **2022**, *7*, 3112.
[10] I. Bardenhagen, O. Yezerska, M. Augustin, D. Fenske, A. Wittstock, M. Bäumer, *J. Power Sources* **2015**, *278*, 255.

© 2025 The Author(s). ChemElectroChem published by Wiley-VCH GmbH

21960216, 2025, 12, Downloaded from https://chemistry-europe.onlinelibrary.wiley.com/doi/10.1002/celc.202500051 by University Of Sao Paulo - Brazil, Wiley Online Library on [24/06/2025]. See the Terms and Conditions (https://onlinelibrary.wiley.com/terms-and-conditions) on Wiley Online Library for rules of use; OA articles are governed by the applicable Creative Commons License

[11] W. Xu, J. Hu, M. H. Engelhard, S. A. Towne, J. S. Hardy, J. Xiao, J. Feng, M. Y. Hu, J. Zhang, F. Ding, M. E. Gross, J.-G. Zhang, *J. Power Sources* **2012**, *215*, 240.
[12] Y. Dou, Z. Xie, Y. Wei, Z. Peng, Z. Zhou, *Natl. Sci. Rev.* **2022**, *9*, nwac040.
[13] L. Johnson, C. Li, Z. Liu, Y. Chen, S. A. Freunberger, P. C. Ashok, B. B. Praveen, K. Dholakia, J.-M. Tarascon, P. G. Bruce, *Nat. Chem.* **2014**, *6*, 1091.
[14] C. J. Allen, J. Hwang, R. Kautz, S. Mukerjee, E. J. Plichta, M. A. Hendrickson, K. M. Abraham, *J. Phys. Chem. C* **2012**, *116*, 20755.
[15] M. J. Trahan, S. Mukerjee, E. J. Plichta, M. A. Hendrickson, K. M. Abraham, *J. Electrochem. Soc.* **2013**, *160*, A259.
[16] Y. Wang, Y.-C. Lu, *Energy Storage Mater.* **2020**, *28*, 235.
[17] G. Huang, J. Wang, X. Zhang, *ACS Cent. Sci.* **2020**, *6*, 2136.
[18] D. M. Josepetti, B. P. Sousa, S. A. J. Rodrigues, R. G. Freitas, G. Doubek, *J. Energy Chem.* **2024**, *88*, 223.
[19] W. Li, M. Zeng, B. Wang, Y. Chen, C. N. Markides, *J. Energy Storage* **2024**, *82*, 110544.
[20] M. T. Rauter, M. Augustin, L. Spitthoff, A. M. Svensson, *J. Appl. Electrochem.* **2021**, *51*, 1437.
[21] R. G. Pearson, *J. Am. Chem. Soc.* **1963**, *85*, 3533.
[22] Y. Zhang, X. Zhang, J. Wang, W. C. McKee, Y. Xu, Z. Peng, *J. Phys. Chem. C* **2016**, *120*, 3690.
[23] Z. Jiang, A. M. Rappe, *J. Am. Chem. Soc.* **2022**, *144*, 22150.
[24] N. B. Aetukuri, B. D. McCloskey, J. M. García, L. E. Krupp, V. Viswanathan, A. C. Luntz, *Nat. Chem.* **2015**, *7*, 50.
[25] B. D. Adams, C. Radtke, R. Black, M. L. Trudeau, K. Zaghib, L. F. Nazar, *Energy Environ. Sci.* **2013**, *6*, 1772.
[26] A. Halder, H.-H. Wang, K. C. Lau, R. S. Assary, J. Lu, S. Vajda, K. Amine, L. A. Curtiss, *ACS Energy Lett.* **2018**, *3*, 1105.
[27] X. Liu, X. Song, Q. Zhang, X. Zhu, Q. Han, Z. Liu, P. Zhang, Y. Zhao, *J. Energy Chem.* **2022**, *69*, 516.
[28] T. Liu, M. Leskes, W. Yu, A. J. Moore, L. Zhou, P. M. Bayley, G. Kim, C. P. Grey, *Science* **2015**, *350*, 530.
[29] A. E. Torres, P. B. Balbuena, *Chem. Mater.* **2018**, *30*, 708.
[30] S. Meini, M. Piana, N. Tsiouvaras, A. Garsuch, H. A. Gasteiger, *Electrochem. Solid-State Lett.* **2012**, *15*, A45.
[31] M. D. Radin, J. F. Rodriguez, F. Tian, D. J. Siegel, *J. Am. Chem. Soc.* **2012**, *134*, 1093.
[32] A. I. Belova, D. G. Kwabi, L. V. Yashina, Y. Shao-Horn, D. M. Itkis, *J. Phys. Chem. C* **2017**, *121*, 1569.
[33] P. Zhang, M. Ding, X. Li, C. Li, Z. Li, L. Yin, *Adv. Energy Mater.* **2020**, *10*, 2001789.
[34] Q. Xiong, C. Li, Z. Li, Y. Liang, J. Li, J. Yan, G. Huang, X. Zhang, *Adv. Mater.* **2022**, *34*, 2110416.
[35] Y. Li, X. Wang, S. Dong, X. Chen, G. Cui, *Adv. Energy Mater.* **2016**, *6*, 1600751.
[36] Z. Zhao, X. Zhang, Z. Zhou, E. Wang, Z. Peng, *Nano Lett.* **2022**, *22*, 501.
[37] C. Zhao, Z. Yan, B. Zhou, Y. Pan, A. Hu, M. He, J. Liu, J. Long, *Angew. Chem., Int. Ed.* **2023**, *62*, e202302746.
[38] R. Zheng, D. Du, Y. Yan, S. Liu, X. Wang, C. Shu, *Adv. Funct. Mater.* **2024**, *34*, 2316440.
[39] H. Xu, R. Zheng, D. Du, L. Ren, R. Li, X. Wen, C. Zhao, T. Zeng, B. Zhou, C. Shu, *Sci. China Mater.* **2022**, *65*, 1761.
[40] D. Du, R. Zheng, X. Chen, W. Xiang, C. Zhao, B. Zhou, R. Li, H. Xu, C. Shu, *ACS Appl. Mater. Interfaces* **2021**, *13*, 33133.
[41] B. P. Sousa, T. C. Lourenço, C. G. Anchieta, T. C. M. Nepel, R. M. Filho, J. L. F. Da Silva, G. Doubek, *Small* **2024**, *20*, 2306895.
[42] J. Read, *J. Electrochem. Soc.* **2002**, *149*, A1190.
[43] P. G. Bruce, S. A. Freunberger, L. J. Hardwick, J.-M. Tarascon, *Nat. Mater.* **2012**, *11*, 19.
[44] C. Liu, K. Sato, X.-B. Han, S. Ye, *Curr. Opin. Electrochem.* **2019**, *14*, 151.
[45] Y. Zhou, S. Guo, *eScience* **2023**, *3*, 100123.
[46] C. Shu, J. Wang, J. Long, H.-K. Liu, S.-X. Dou, *Adv. Mater.* **2019**, *31*, 1804587.
[47] T. Ogasawara, A. Débart, M. Holzapfel, P. Novák, P. G. Bruce, *J. Am. Chem. Soc.* **2006**, *128*, 1390.
[48] Y.-C. Lu, Y. Shao-Horn, *J. Phys. Chem. Lett.* **2013**, *4*, 93.
[49] S. Kang, Y. Mo, S. P. Ong, G. Ceder, *Chem. Mater.* **2013**, *25*, 3328.
[50] Y.-C. Lu, B. M. Gallant, D. G. Kwabi, J. R. Harding, R. R. Mitchell, M. S. Whittingham, Y. Shao-Horn, *Energy Environ. Sci.* **2013**, *6*, 750.
[51] Y. Wang, N.-C. Lai, Y.-R. Lu, Y. Zhou, C.-L. Dong, Y.-C. Lu, *Joule* **2018**, *2*, 2364.
[52] N. Meethong, H.-Y. S. Huang, S. A. Speakman, W. C. Carter, Y.-M. Chiang, *Adv. Funct. Mater.* **2007**, *17*, 1115.
[53] M. D. Levi, D. Aurbach, *J. Solid State Electrochem.* **2007**, *11*, 1031.
[54] W. Simons, D. Gonnissen, A. Hubin, *J. Electroanal. Chem.* **1997**, *433*, 141.
[55] S. Ganapathy, B. D. Adams, G. Stenou, M. S. Anastasaki, K. Goubitz, X.-F. Miao, L. F. Nazar, M. Wagemaker, *J. Am. Chem. Soc.* **2014**, *136*, 16335.
[56] S. T. Plunkett, H.-H. Wang, S. H. Park, Y. J. Lee, J. Cabana, K. Amine, S. Al-Hallaj, B. P. Chaplin, L. A. Curtiss, *ACS Appl. Energy Mater.* **2020**, *3*, 12575.
[57] F. Cai, X. Lei, Q. Ke, C. Ouyang, *J. Phys. Chem. C* **2023**, *127*, 14232.
[58] J. Wang, R. Gao, X. Liu, *Inorganics* **2023**, *11*, 69.
[59] W. Yu, Z. Shen, T. Yoshii, S. Iwamura, M. Ono, S. Matsuda, M. Aoki, T. Kondo, S. R. Mukai, S. Nakanishi, H. Nishihara, *Adv. Energy Mater.* **2024**, *14*, 2303055.
[60] B. J. Bergner, A. Schürmann, K. Peppler, A. Garsuch, J. Janek, *J. Am. Chem. Soc.* **2014**, *136*, 15054.
[61] K. Nishioka, M. Tanaka, H. Fujimoto, T. Amaya, S. Ogoshi, M. Tobisu, S. Nakanishi, *Angew. Chem., Int. Ed.* **2022**, *61*, e202112769.
[62] D. Córdoba, H. B. Rodríguez, E. J. Calvo, *J. Phys. Chem. C* **2023**, *127*, 78.
[63] N. Mahne, B. Schafzahl, C. Leypold, M. Leypold, S. Grumm, A. Leitgeb, G. A. Strohmeier, M. Wilkening, O. Fontaine, D. Kramer, C. Slugovc, S. M. Borisov, S. A. Freunberger, *Nat. Energy* **2017**, *2*, 1.
[64] S. Ahn, C. Zor, S. Yang, M. Lagnoni, D. Dewar, T. Nimmo, C. Chau, M. Jenkins, A. J. Kibler, A. Pateman, G. J. Rees, X. Gao, P. Adamson, N. Grobert, A. Bertei, L. R. Johnson, P. G. Bruce, *Nat. Chem.* **2023**, *15*, 1022.
[65] H.-D. Lim, B. Lee, Y. Bae, H. Park, Y. Ko, H. Kim, J. Kim, K. Kang, *Chem. Soc. Rev.* **2017**, *46*, 2873.
[66] J. Hassoun, F. Croce, M. Armand, B. Scrosati, *Angew. Chem., Int. Ed.* **2011**, *50*, 2999.
[67] J. Park, S. H. Lee, H. Jung, D. Aurbach, Y. Sun, *Adv. Mater.* **2018**, *30*, 1704162.
[68] Y. Qiao, Y. He, S. Wu, K. Jiang, X. Li, S. Guo, P. He, H. Zhou, *ACS Energy Lett.* **2018**, *3*, 463.
[69] A. Y. Tesio, W. Torres, M. Villalba, F. Davia, M. del Pozo, D. Córdoba, F. J. Williams, E. J. Calvo, *ChemElectroChem* **2022**, *9*, e202201037.
[70] S. Xing, Z. Zhang, Y. Dou, M. Li, J. Wu, Z. Zhang, Z. Zhou, *CCS Chem.* **2023**, *6*, 1810.
[71] H.-W. Lee, H. Kim, H.-G. Jung, Y.-K. Sun, W.-J. Kwak, *Adv. Funct. Mater.* **2021**, *31*, 2102442.
[72] Y. G. Zhu, X. Wang, C. Jia, J. Yang, Q. Wang, *ACS Catal.* **2016**, *6*, 6191.
[73] X. Wu, X. Wang, Z. Li, L. Chen, S. Zhou, H. Zhang, Y. Qiao, H. Yue, L. Huang, S.-G. Sun, *Nano Lett.* **2022**, *22*, 4985.
[74] X. Cui, Y. Luo, Y. Zhou, W. Dong, W. Chen, *Nanotechnology* **2021**, *32*, 132003.
[75] Z. Jiang, Y. Huang, Z. Zhu, S. Gao, Q. Lv, F. Li, *Proc. Natl. Acad. Sci.* **2022**, *119*, e2202835119.
[76] Z. Jiang, B. Wen, Y. Huang, Y. Guo, Y. Wang, F. Li, *Angew. Chem., Int. Ed.* **2024**, *63*, e202315314.
[77] Y. Lin, Q. Yang, F. Geng, H. Feng, M. Chen, B. Hu, *J. Phys. Chem. Lett.* **2021**, *12*, 10346.
[78] Z. Lacour, Y. Ham, L. Brazel, C. P. Grey, I. Temprano, *Chem. Commun.* **2025**, *61*, 2516.
[79] J. Wandt, P. Jakes, J. Granwehr, H. A. Gasteiger, R.-A. Eichel, *Angew. Chem., Int. Ed.* **2016**, *55*, 6892.
[80] Y. K. Petit, E. Mourad, C. Prehal, C. Leypold, A. Windischbacher, D. Mijailovic, C. Slugovc, S. M. Borisov, E. Zojer, S. Brutti, O. Fontaine, S. A. Freunberger, *Nat. Chem.* **2021**, *13*, 465.
[81] E. Mourad, Y. K. Petit, R. Spezia, A. Samojlov, F. F. Summa, C. Prehal, C. Leypold, N. Mahne, C. Slugovc, O. Fontaine, S. Brutti, S. A. Freunberger, *Energy Environ. Sci.* **2019**, *12*, 2559.
[82] Q. Lv, Z. Zhu, S. Zhao, L. Wang, Q. Zhao, F. Li, L. A. Archer, J. Chen, *J. Am. Chem. Soc.* **2021**, *143*, 1941.
[83] B. Wen, Y. Huang, Z. Jiang, Y. Wang, W. Hua, S. Indris, F. Li, *Adv. Mat.* **2024**, *36*, 2405440.
[84] M. Zhu, M. Li, Y. Lian, X. Guo, J. Liu, P. Ma, L. Xiao, *J. Phys. Chem. C* **2022**, *126*, 10248.

Manuscript received: February 5, 2025
Revised manuscript received: March 29, 2025
Version of record online: May 12, 2025

© 2025 The Author(s). ChemElectroChem published by Wiley-VCH GmbH

21960216, 2025, 12, Downloaded from https://chemistry-europe.onlinelibrary.wiley.com/doi/10.1002/celc.202500051 by University Of Sao Paulo - Brazil, Wiley Online Library on [24/06/2025]. See the Terms and Conditions (https://onlinelibrary.wiley.com/terms-and-conditions) on Wiley Online Library for rules of use; OA articles are governed by the applicable Creative Commons License